Nano Energy 107 (2023) 108160

Contents lists available at ScienceDirect

Nano Energy

journal homepage: www.elsevier.com/locate/nanoen

Simultaneous solar-driven seawater desalination and continuous oil recovery

Shiwen Wu [a], Ruda Jian [a], Siyu Tian [a], Long Zhou [a], Tengfei Luo [b], Guoping Xiong [a,*]

[a] Department of Mechanical Engineering, The University of Texas at Dallas, Richardson, TX 75080, USA
[b] Department of Aerospace and Mechanical Engineering, University of Notre Dame, Notre Dame, IN 46556, USA

ARTICLE INFO

Keywords:
Simultaneous
Seawater desalination
Oil recovery
Solar energy
Siphon effect

ABSTRACT

Oil spills and freshwater scarcity remain two worldwide challenging issues. Emerging efforts have been made either to recover oil from oil/water mixture or to extract freshwater from abundant seawater. However, almost all current devices focus on oil recovery or seawater desalination separately, which is lack of energy efficiency. Herein, we propose a design of mechanically robust, bi-functional graphene devices (BGDs), containing vertical graphene sheets decorated on inverted U-shaped graphene monoliths, to achieve simultaneous solar-driven vapor generation and continuous oil recovery from oil-contaminated seawater. Benefiting from the unique wettability design of the BGDs, water evaporates on the hydrophilic surfaces, and meanwhile oil can be spontaneously recovered through the hydrophobic/oleophilic interior channels due to siphon action. Moreover, the strong photothermal effect of vertical graphene can boost both the seawater desalination and oil recovery performance. As a result, a vapor generation rate of 2.04 kg m^{-2} h^{-1} and an oil recovery rate of 105.8 L m^{-2} h^{-1} are concurrently achieved under 1-sun irradiation. The design of bi-functional devices provides a new means to maximize the utilization of solar power and reduce the costs for multi-functional practical environmental engineering applications.

Oil leakage during offshore oil production or marine transportation has not only led to tremendous loss of valuable oil resource, but also resulted in severe pollution to seawater [1]. Meanwhile, seawater covers over 70% of the Earth surface, providing sufficient content of feedwater for generating freshwater to address the water scarcity issue all over the world [2]. Over the past few decades, continuous efforts have been made to either recover oil from the oil/water mixture such as physical adsorption [3,4] and skimmer vessels [5], or desalinate seawater to obtain freshwater such as reverse osmosis [6] and solar desalination [7,8]. However, almost all these technologies focus on oil recovery or seawater desalination separately, leading to unavoidable energy losses. Moreover, conventional devices generating vapor from oil-containing wastewater generally suffer from oil fouling issues [9]. Multi-functional devices, meeting the demands of different applications simultaneously, are needed to further improve the overall energy utilization and reduce equipment costs [10–12] to resolve the environmental and oceanographic issues.

Recently, we have developed a series of siphon-enabled oil skimmers to continuously recover oil from oil-contaminated wastewater [13,14] without the need for expensive complex equipment and human intervention. These oil skimmers exhibited excellent solar absorption performance, facilitating the reduction of oil viscosity because of the solar-heating effect and thus significantly enhancing the oil recovery rate. Meanwhile, thermal energy converted from sunlight has also been widely employed to vaporize the abundant seawater to obtain drinkable freshwater in prior work [15–19]. This inspires us to develop integrated, bi-functional devices that can adopt solar energy to achieve simultaneous vapor generation and oil recovery from oil-contaminated seawater. As such, the heat conduction loss in individual applications (e.g., solar vapor generation) can be avoided and utilized in the other one, maximizing the value of the limited solar energy input and reducing the equipment costs.

In this paper, we propose the design of mechanically robust bi-functional graphene devices (BGDs) to achieve simultaneously high solar-driven vapor generation and continuous oil recovery performance. As schematically illustrated in Fig. 1, an inverted U-shape BGD, with the surface partially treated to be hydrophilic and the interior remaining hydrophobic/oleophilic, is employed to simultaneously generate vapor and recover oil from oil-contaminated seawater. Benefiting from the unique structural and wettability design, seawater can be wicked to the

* Corresponding author.
E-mail address: guoping.xiong@utdallas.edu (G. Xiong).

https://doi.org/10.1016/j.nanoen.2022.108160
Received 3 October 2022; Received in revised form 14 December 2022; Accepted 28 December 2022
Available online 30 December 2022

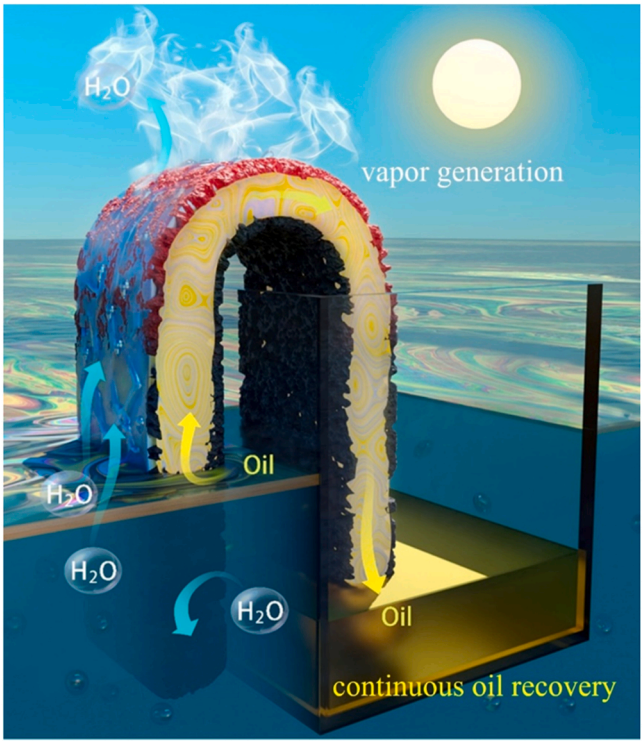

Fig. 1. Schematic illustration of solar-driven simultaneous vapor generation and continuous oil recovery from oil-contaminated seawater by the BGDs.

hydrophilic surfaces by capillary force and thus evaporates therein, and meanwhile oil can be continuously recovered through the hydrophobic/oleophilic interior channels due to siphon action. Moreover, sunlight can be effectively captured and converted into thermal energy by the BGDs, enabling fast solar-driven vapor generation and enhanced oil recovery because of the reduced oil viscosity. Consequently, a vapor generation rate of 2.04 kg m^{-2} h^{-1} and an oil recovery rate of 105.8 L m^{-2} h^{-1} are concurrently achieved under 1-sun irradiation (i.e., solar irradiance of 1 kW m^{-2}), exhibiting great potential for practical environmental engineering applications such as oil-contaminated seawater treatment without any consumption of external power such as electricity or manual intervention.

The BGDs are prepared with details described in Supplementary Materials. Briefly, an inverted U-shape graphene monolith (GM) is fabricated via a mold-assisted freeze-casting process. The as-obtained GM possesses massive micro-sized pores acting as channels for continuous oil transport (Supplementary Fig. S2). Subsequently, graphene petals (GPs) are grown on the surface of GMs through plasma-enhanced chemical vapor deposition (PECVD) to enhance the capability of solar absorption (Supplementary Fig. S3). The GP/GM samples are then coated by a sub-micron-thick polydimethylsiloxane (PDMS) layer (Supplementary Fig. S4) to obtain the BGDs. The BGDs are naturally hydrophobic and oleophilic because of the thin layer coating of PDMS (Supplementary Fig. S5). Scanning electron microscopy (SEM) image in Fig. 2a shows that the porous structure of GM can be well maintained after the coating process. Meanwhile, the BGDs exhibit strong mechanical stability due to the protection from the PDMS coating. Fig. 2b presents the stress-strain curves of a typical BGD at different compressive strains. The BGD shows maximum stresses of 2.45 and 46.67 kPa when applying 10% and 90% compressive strains, respectively, and the height can be fully recovered even after the 90% compressive test. In contrast, the height of a typical GP/GM control sample without PDMS coating can only be recovered to 35% of the initial value after the 90% compressive test (Supplementary Fig. S6). Furthermore, the BGD exhibits excellent stress and shape recoveries over 100 compression cycles (Fig. 2c). The height of the BGD remains almost unchanged compared to the initial state, and the maximum stress retains 81% of its initial value after 100 compression cycles. Fig. 2d displays the absorbance spectrum of the BGDs within the solar spectrum with an average absorptivity of 99%, demonstrating the strong light absorption capability due to the light-trapping effect of GPs [13,20,21]. Consequently, solar energy can be efficiently absorbed by the BGDs and converted to thermal energy, which can not only enhance the vapor generation rate but also facilitate oil transport by reducing the viscosity of oil [13,14].

The wettability of the BGDs is selectively controlled by air plasma treatment to realize the bi-functionality of solar vapor generation and continuous oil recovery. Details of the plasma treatment procedure are

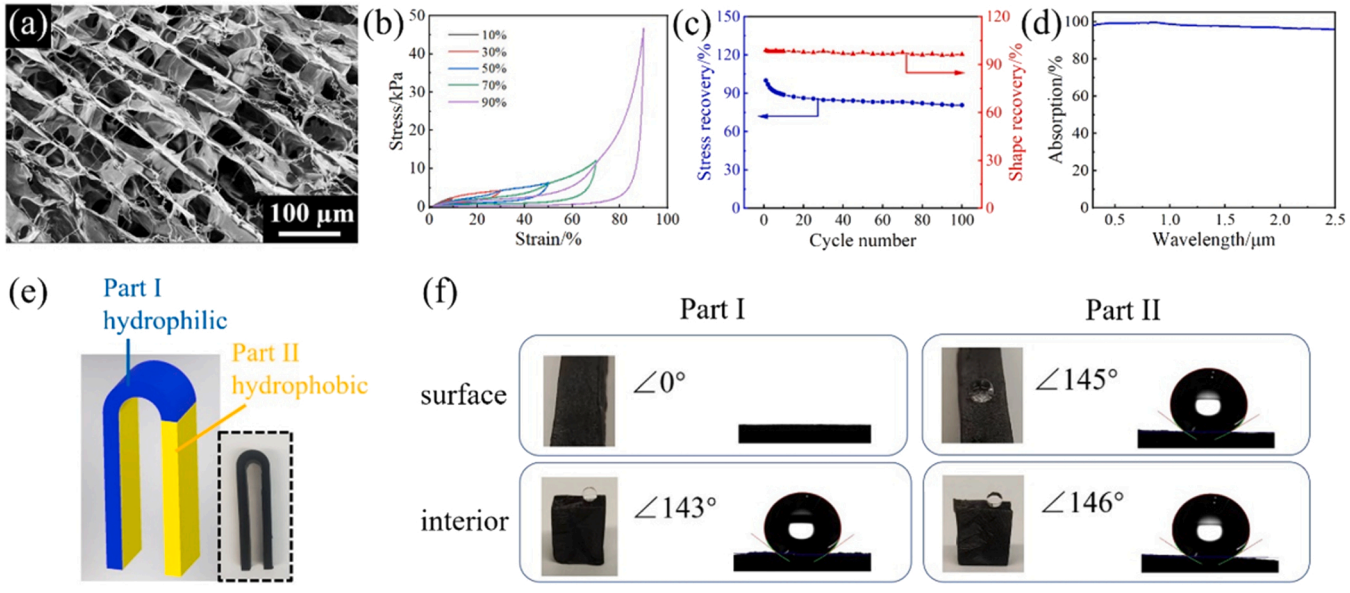

Fig. 2. (a) SEM image showing the porous structure of the BGDs. (b) Stress-strain curves of a typical BGD at different compressive strains. (c) Mechanical stability of the BGD over 100 loading-unloading cycles. (d) Absorption curves of the BGDs within the solar spectrum. (e) Schematic showing the wettability of the BGDs after plasma treatment. Inset displays an optical image of the BGD. (f) Water contact angle measurements at part I and part II of the BGDs. The surfaces of part I become hydrophilic after plasma treatment, while the surfaces of part II and the interiors of part I and part II remain hydrophobic.

shown in Supplementary Note S1. As shown in Fig. 2e and Supplementary Fig. S7, different plasma treatment conditions are applied to the two parts of the BGDs. Part I is exposed to the plasma environment, while part II is protected by a shield during the plasma treatment. After the treatment for a duration of 60 s, the surfaces of part I thus become hydrophilic, while the surfaces of part II and the interior of both parts I and II remain hydrophobic, as demonstrated by the water contact angle measurements shown in Fig. 2f. Water contact angle hysteresis on part II is also measured and calculated to be $14.9 \pm 2.0^{\circ}$, indicating weak adsorption of water on the parts of BGDs without plasma treatment [22–24] (Supplementary Fig. S8). The excellent water transport capacity of the plasma-treated surface is also illustrated by the capillary rise test, which shows that water can climb up to 5 cm in 49 s on the surface with plasma treatment (Supplementary Fig. S9 and Supplementary Video S1). The duration of plasma treatment is carefully controlled to obtain a thin hydrophilic layer on the surface of part I as water pathways for vapor generation and at the same time allow oil to flow through the interior channels. As a result, water can spread over the surfaces of part I due to capillary force and evaporate therein; meanwhile oil can flow through the hydrophobic/oleophilic channels of part I and part II, and reach the collecting chamber due to siphon action.

Supplementary material related to this article can be found online at doi:10.1016/j.nanoen.2022.108160.

Next, the bi-functionality of simultaneous solar-driven vapor generation and oil recovery of the BGDs is demonstrated. Fig. 3a exhibits a schematic of the experimental setup, containing two chambers separated by a wall. A mineral oil/water mixture with a volume ratio of oil to water = 1:2 is added to the left chamber to mimic the oil-contaminated wastewater. The plasma-treated BGDs are placed on top of the separating wall to connect the two chambers. The content of evaporated water can be characterized by the mass change of the entire setup; meanwhile the recovered oil can flow along the BGDs to the right

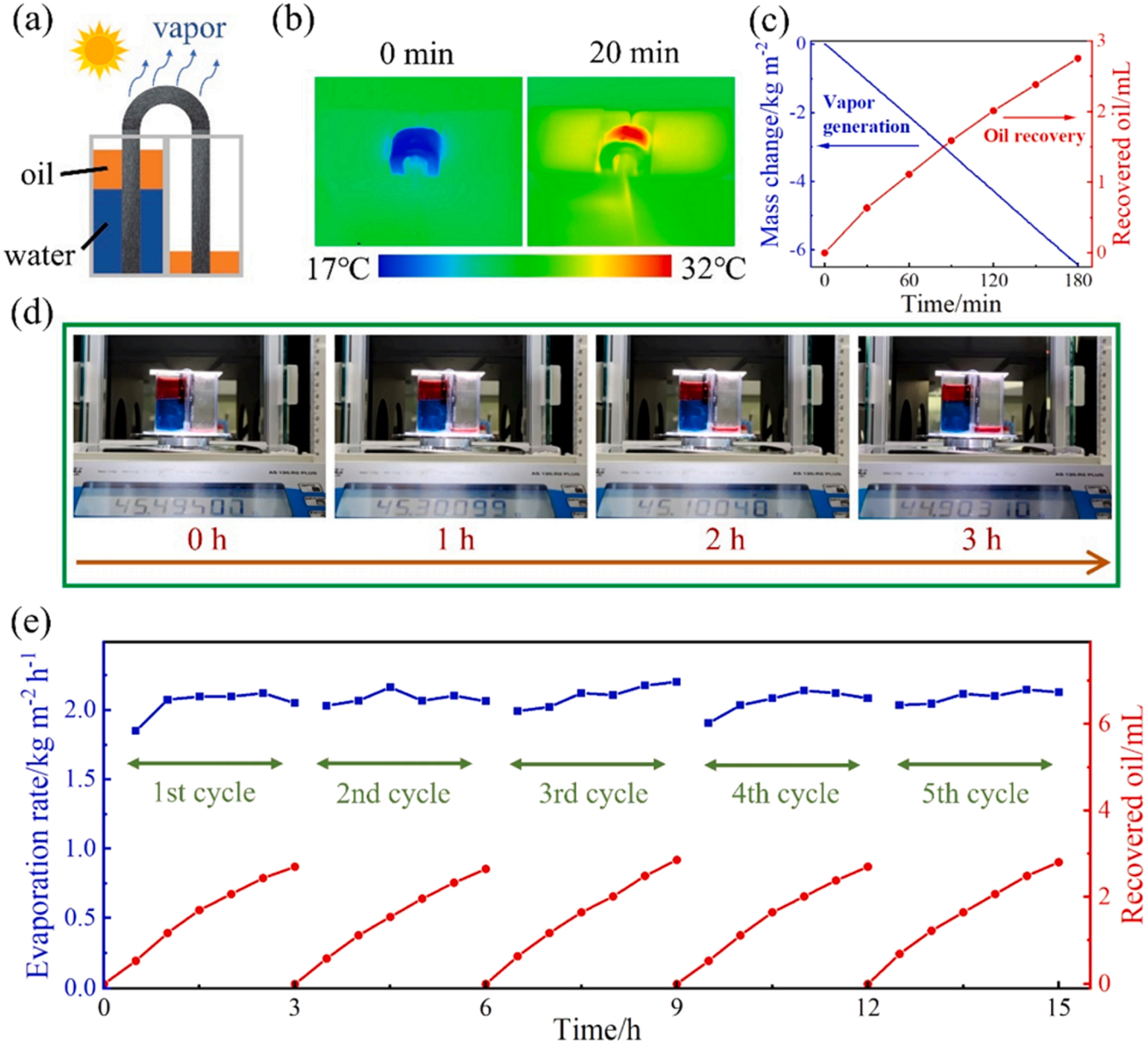

Fig. 3. (a) Schematic illustration of the test setup for solar-driven simultaneous vapor generation and oil recovery. The blue color represents water. The orange color represents mineral oil. (b) IR images exhibiting the surface temperature change of the BGD working at 1 sun. (c) Mass evolution of evaporated water and volume evolution of recovered oil by the BGD working at 1 sun. (d) Optical images showing the simultaneous vapor generation and oil recovery process enabled by the BGD at 1 sun. The decreasing weight of the entire setup is caused by water evaporation. (e) Cyclic stability of the BGD working under 1 sun.

chamber due to siphon action, and the oil flow rate can thus be determined. When exposed to the simulated sunlight, both chambers are covered to ensure that only the top surface of the BGD is illuminated. Fig. 3b shows the surface temperature evolution of the BGD under 1 sun of solar illumination. When solar illumination is off, the surface temperature of the BGD is significantly lower than the ambient temperature because of the evaporative cooling effect. The temperature of the top BGD surface rises to 32 ℃ within 20 min after the solar simulator is turned on, which can be attributed to the outstanding solar absorption property and solar-heating effect of GPs. The promoted temperature of GPs can not only enhance the vapor generation rate but also facilitate the oil recovery process because of the reduced oil viscosity [13,14].

The simultaneous vapor generation and oil recovery performance of the BGDs are evaluated (Fig. 3c) by recording the processes using a digital camera (Fig. 3d and Supplementary Video S2). Results show that a typical BGD exhibits bi-functional vapor generation and oil recovery capabilities with a vapor generation rate of 2.04 ± 0.09 kg m^{-2} h^{-1} and an oil recovery rate of 105.8 ± 9.3 L m^{-2} h^{-1} simultaneously achieved under 1 sun of solar illumination. Both vapor generation rate and oil recovery rate are enhanced compared to those (vapor generation rate of 0.69 ± 0.04 kg m^{-2} h^{-1} and an oil recovery rate of 70.5 ± 6.8 L m^{-2} h^{-1}, Supplementary Fig. S10) under dark conditions, indicating that the absorbed solar energy has been utilized concurrently in the two integrated applications. The energy efficiency of solar-driven vapor generation (η) can be calculated by [17,25]:

$$\eta = \frac{\Delta m[L_v + c(T_1 - T_0)]}{\alpha P} \quad (1)$$

where Δm represents the difference in evaporation rate under 1 sun of solar irradiation and dark conditions. $L_v = 1.91846 \times 10^6[T_1/(T_1 - 33.91)]^2$ J kg^{-1} is the evaporation enthalpy of water. c= 4.2 J g^{-1} K^{-1} is the specific heat capacity of water. T_1 and T_0 represent the average surface temperature and bulk temperature of water, respectively. P is the solar irradiation power (1 kW m^{-2} in this work), and α is the weighed solar absorption of the BGDs which is calculated to be 99% through the absorbance spectrum in Fig. 2d. As a result, the energy efficiency of vapor generation by the BGDs under 1 sun of solar irradiation is calculated to be 93%. Moreover, the separation efficiency of oil recovery from oil/water mixture in the left chamber is calculated to be 99.85% (Supplementary Fig. S11), indicating the excellent oil recovery performance of the BGDs.

Supplementary material related to this article can be found online at doi:10.1016/j.nanoen.2022.108160.

Similar tests are conducted with control samples to illustrate the effectiveness of the unique wettability design of the BGDs on achieving the bi-functionality of simultaneous vapor generation and oil recovery. For the control samples without plasma treatment, oil in the left chamber can be recovered while almost no water is evaporated during 4-h continuous solar illumination at 1 sun (Supplementary Fig. S12). In contrast, for the control samples with the entire surfaces treated by plasma (i.e., without shield during plasma treatment), both water and oil can be transferred to the right chamber because of siphon action (Supplementary Fig. S13), failing to extract oil from the oil-contaminated wastewater. The performance of the BGDs is also compared with that when vapor generation and oil recovery are realized separately. A water evaporation rate of 2.05 ± 0.02 kg m^{-2} h^{-1} is achieved when the BGDs is working with pure water (Supplementary Fig. S14), closed to the water evaporation rate of the BGDs working as bi-functional devices (i.e., 2.04 kg m^{-2} h^{-1}), indicating that simultaneously recovering oil and generating vapor will not sacrifice the water evaporation performance of the BGDs. On the other hand, an oil recovery rate of 147.1 ± 5.1 L m^{-2} h^{-1} can be achieved when the BGDs are only recovering oil (Supplementary Fig. S12), which is higher than the value (i.e., 105.8 L m^{-2} h^{-1}) when the BGDs realize both functions, because water evaporation will consume part of the absorbed solar energy. Here we compare the performance of the BGDs with relevant devices reported in prior work (Supplementary Tables S1–3). The evaporation rate of the BGDs at 1 sun is superior to most of the reported bi-functional devices and is comparable to those solar desalination devices treating 3.5 wt% NaCl solutions. The oil recovery rate of the BGDs (i.e., 105.8 L m^{-2} h^{-1}) is comparable to that of our prior reported siphon-assisted oil skimmers (123.3 L m^{-2} h^{-1}). This value is lower than that of conventional electricity-powered oil recovery devices (see Supplementary Table S3). Nevertheless, oil recovery by those conventional devices requires complex equipment such as pumps and heaters, leading to undesirable complex equipment costs, large energy consumption, and continuous human intervention. In contrast, our proposed BGDs rely only on gravitational potential energy difference and renewable solar energy to continuously recover oil, which compensates the slower oil recovery rate by the advantages of economic and energetic costs. The oil recovery rate can also be further enhanced by optimizing the geometry, surface chemistry of the channels and increasing the height difference [13,14] in the future work. Moreover, we also note that simultaneously recovering oil and generating vapor by the BGDs will not sacrifice the water evaporation performance of the BGDs (Supplementary Fig. S14).

Oil recovery tests based on another type of oil with much higher viscosities (151.2 mPa s at 25 ℃) are conducted on the BGDs (Supplementary Fig. S15). Results show that simultaneous vapor generation and oil recovery can also be achieved when treating high-viscosity oils, indicating that the proposed BGDs are capable to treat water contaminated by oil with a wide range of viscosities. Cyclic stability is another crucial factor determining the overall performance of the BGDs in practical applications. We conduct a 5-cycle test on the vapor generation and oil recovery performance of the BGDs under 1-sun irradiation, as shown in Fig. 3e. Both vapor generation rate and oil recovery rate remain relatively stable, indicating the excellent cyclic stability of the BGDs.

During the treatment of practical oil-contaminated seawater, salt crystals may precipitate and accumulate on evaporating surfaces, blocking the absorption of sunlight and leading to significant deterioration of the performance. Therefore, we further evaluate the anti-salt fouling performance of the BGDs. Herein, a continuous 24-h test is conducted under 1-sun irradiation with oil and 3.5 wt% NaCl solution mixture (mimicking the oil-contaminated seawater) initially placed in the left chamber. Since the oil recovery performance depends largely on the height difference between the upper surfaces of oil in the left and right chambers [13], we manually transfer the collected oil in the right chamber to the left one every 4 h. As shown in Fig. 4a, the evaporation rate remains stable during the 24-h test, and the volume of recovered oil remains almost unchanged for every 4-h operating period. Fig. 4b contains photographs of the BGD top surface at different times during the 24-h test to reveal the evolution of precipitated salts. Apparently, the salts preferentially accumulate at the interface between part I and part II (i.e., the boundaries between hydrophilic and hydrophobic regions) in BGDs, leaving the main top surface clean and directly exposed to solar illumination and thus achieving the excellent anti-salt fouling performance. Such unique anti-salt fouling properties can be attributed to the Marangoni effect [26]. NaCl solutions are continuously driven to the interfaces between part I and part II by a combination of evaporation-induced and Marangoni flows, leading to preferential accumulation of salt crystals at the interfaces [26]. Moreover, the precipitated salt can be easily removed by gentle touch (Supplementary Fig. S16 and Video S3), with the precipitation rate calculated to be 57.1 g m^{-2} h^{-1}.

Supplementary material related to this article can be found online at doi:10.1016/j.nanoen.2022.108160.

To demonstrate the water purification capability during the solar desalination process, we collect the purified water by condensing the generated vapor during solar desalination through the BGDs. The methyl blue-dyed 3.5 wt% NaCl solution is transformed to clear and colorless water after purification by the BGDs (Fig. 4c). Furthermore, the qualities

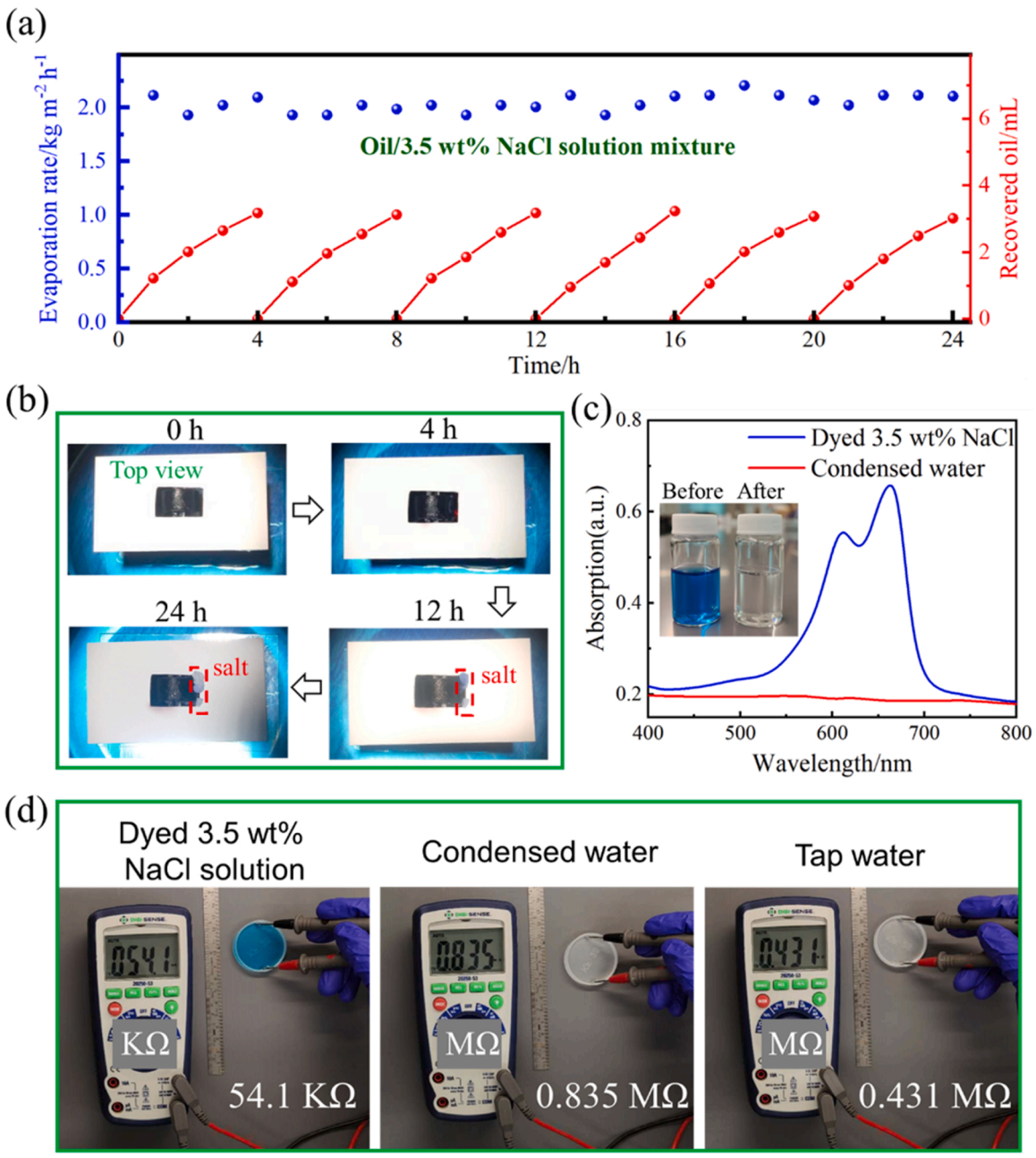

Fig. 4. (a) Vapor generation and oil recovery performance of the BGD working with a solution mixture of mineral oil/3.5 wt% NaCl. The collected oil in the right chamber is transferred to the left one every 4 h. (b) Photographs of the BGD top surface at different times during the 24-h test. (c) UV–vis spectra of the dyed 3.5 wt% NaCl solution and purified water. Insert image shows the photographs of the dyed 3.5 wt% NaCl solution (left) and purified water (right). (d) The electrical resistances of methyl blue-dyed 3.5 wt% NaCl solution, condensed water, and tap water measured by a multimeter with a constant distance between its two electrodes.

of different water samples are evaluated by measuring the electrical resistance using a multimeter with a constant distance between two electrodes [27–29]. The electrical resistances of the dyed 3.5 wt% NaCl solution, condensed water and tap water are measured to be 0.054 MΩ, 0.835 MΩ and 0.431 MΩ, respectively (Fig. 4d), suggesting that the dyed 3.5 wt% NaCl solution has been effectively purified by the BGDs. In addition to oil/water mixtures, the BGDs are also applicable to treat oil-water emulsions with a separation efficiency of up to 99.19% (Supplementary Figs. S11 and S17).

In summary, mechanically robust BGDs are designed to achieve solar-driven simultaneous vapor generation and continuous oil recovery from oil-contaminated seawater. By controlling the wettability of the BGDs, seawater can be pumped to the hydrophilic surfaces by capillary force and evaporate therein, meanwhile oil can flow through the hydrophobic/oleophilic interior channels and be recovered via a siphon-assisted self-pumping process. Moreover, solar energy can be effectively absorbed and converted into thermal energy by GPs on BGDs, leading to simultaneously enhanced vapor generation and oil recovery rates. Consequently, a vapor generation rate of 2.04 kg m^{-2} h^{-1} and an oil recovery rate of 105.8 L m^{-2} h^{-1} are concurrently achieved under 1-sun irradiation. The proposed design of bi-functional devices provides a novel means to maximize the utilization of solar power towards practical multi-functional environmental engineering applications.

CRediT authorship contribution statement

Shiwen Wu: Conceptualization, Methodology, Investigation, Formal analysis, Writing – original draft. **Ruda Jian:** Investigation, Validation.

Siyu Tian: Investigation, Visualization. **Long Zhou:** Investigation. **Tengfei Luo:** Writing – review & editing. **Guoping Xiong:** Funding acquisition, Supervision, Conceptualization, Writing – review & editing.

Declaration of Competing Interest

The authors declare that they have no known competing financial interests or personal relationships that could have appeared to influence the work reported in this paper.

Data Availability

Data will be made available on request.

Acknowledgements

G.X. thanks the University of Texas at Dallas startup fund and the support from the NSF (Grant No. CBET-1937949, CBET-1949962 and CMMI-1923033). T.L. thanks the support from the NSF (Grant No. CBET-1937923 and CBET-1949910). The authors thank Dr. Rodrigo A. Bernal and Dr. S. M. You for the help and discussion involved in this work.

Appendix A. Supporting information

Supplementary data associated with this article can be found in the online version at doi:10.1016/j.nanoen.2022.108160.

References

[1] A. Jernelöv, Nature 466 (2010) 182–183.
[2] U.P.U. Kunjaram, H. Song, Y. Liu, B.K. Booker, T.J. Cooke, Q. Gan, EcoMat 4 (2022), e12168.
[3] L. Chen, R. Du, J. Zhang, T. Yi, J. Mater. Chem. A 3 (2015) 20547–20553.
[4] Y. Shi, B. Wang, S. Ye, Y. Zhang, B. Wang, Y. Feng, W. Han, C. Liu, C. Shen, Appl. Surf. Sci. 535 (2021), 147690.
[5] J. Ge, H.-Y. Zhao, H.-W. Zhu, J. Huang, L.-A. Shi, S.-H. Yu, Adv. Mater. 28 (2016) 10459–10490.
[6] G. He, Y. Zhao, J. Wang, H. Li, Y. Zhu, S. Jiang, Int. J. Water Resour. Dev. 35 (2019) 587–604.
[7] Z. Wang, T. Horseman, A.P. Straub, N.Y. Yip, D. Li, M. Elimelech, S. Lin, Sci. Adv. 5 (2019) eaax0763.
[8] Y. Pang, J. Zhang, R. Ma, Z. Qu, E. Lee, T. Luo, ACS Energy Lett. 5 (2020) 437–456.
[9] S. Wu, B. Gong, H. Yang, Y. Tian, C. Xu, X. Guo, G. Xiong, T. Luo, J. Yan, K. Cen, Z. Bo, K.K. Ostrikov, T.S. Fisher, ACS Appl. Mater. Interfaces 12 (2020) 38512–38521.
[10] A. Dreos, K. Börjesson, Z. Wang, A. Roffey, Z. Norwood, D. Kushnir, K. Moth-Poulsen, Energy Environ. Sci. 10 (2017) 728–734.
[11] M. Gao, P.K.N. Connor, G.W. Ho, Energy Environ. Sci. 9 (2016) 3151–3160.
[12] P. Yang, K. Liu, Q. Chen, J. Li, J. Duan, G. Xue, Z. Xu, W. Xie, J. Zhou, Energy Environ. Sci. 10 (2017) 1923–1927.
[13] S. Wu, S. Tian, R. Jian, T.-N. Wu, T.D. Milazzo, T. Luo, G. Xiong, J. Mater. Chem. A 10 (2022) 11651–11658.
[14] S. Wu, H. Yang, G. Xiong, Y. Tian, B. Gong, T. Luo, T.S. Fisher, J. Yan, K. Cen, Z. Bo, K.K. Ostrikov, ACS Nano 13 (2019) 13027–13036.
[15] Y. Zhang, H. Zhang, T. Xiong, H. Qu, J.J. Koh, D.K. Nandakumar, J. Wang, S. C. Tan, Energy Environ. Sci. 13 (2020) 4891–4902.
[16] F. Nawaz, Y. Yang, S. Zhao, M. Sheng, C. Pan, W. Que, J. Mater. Chem. A 9 (2021) 16233–16254.
[17] Y. Bu, Y. Zhou, W. Lei, L. Ren, J. Xiao, H. Yang, W. Xu, J. Li, J. Mater. Chem. A 10 (2022) 2856–2866.
[18] X. Chen, S. He, M.M. Falinski, Y. Wang, T. Li, S. Zheng, D. Sun, J. Dai, Y. Bian, X. Zhu, J. Jiang, L. Hu, Z.J. Ren, Energy Environ. Sci. 14 (2021) 5347–5357.
[19] L. Zhu, L. Sun, H. Zhang, H. Aslan, Y. Sun, Y. Huang, F. Rosei, M. Yu, Energy Environ. Sci. 14 (2021) 2451–2459.
[20] S. Wu, G. Xiong, H. Yang, B. Gong, Y. Tian, C. Xu, Y. Wang, T. Fisher, J. Yan, K. Cen, T. Luo, X. Tu, Z. Bo, K. (Ken) Ostrikov, Adv. Energy Mater. 9 (2019), 1901286.
[21] S. Wu, G. Xiong, H. Yang, Y. Tian, B. Gong, H. Wan, Y. Wang, T.S. Fisher, J. Yan, K. Cen, Z. Bo, K. (Ken) Ostrikov, Matter 1 (2019) 1017–1032.
[22] K.-Y. Law, Acc. Mater. Res. 3 (2022) 1–7.
[23] T. Huhtamäki, X. Tian, J.T. Korhonen, R.H.A. Ras, Nat. Protoc. 13 (2018) 1521–1538.
[24] J. Drelich, Surf. Innov. 1 (2013) 248–254.
[25] S. Wu, S. Tian, R. Jian, L. Zhou, T. Luo, G. Xiong, Desalination 546 (2023), 116197.
[26] Y. Shao, A. Shen, N. Li, L. Yang, J. Tang, H. Zhi, D. Wang, G. Xue, ACS Appl. Mater. Interfaces 14 (2022) 30324–30331.
[27] Y. Guo, F. Zhao, X. Zhou, Z. Chen, G. Yu, Nano Lett. 19 (2019) 2530–2536.
[28] W. Li, X. Li, J. Liu, M. Zeng, X. Feng, X. Jia, Z.-Z. Yu, ACS Appl. Mater. Interfaces 13 (2021) 22845–22854.
[29] Z. Sun, J. Wang, Q. Wu, Z. Wang, Z. Wang, J. Sun, C.-J. Liu, Adv. Funct. Mater. 29 (2019), 1901312.

Shiwen Wu received his B. S. degree in 2015 and M. S. degree in 2018 from Central South University. Currently he is a PhD candidate in Dr. Guoping Xiong's lab at the University of Texas at Dallas. His current research focuses on solar energy harvesting, fluid transport, thermal management, and 2D materials synthesis.

Ruda Jian, received his B. S. degree from Shandong University of Energy and Environment System Engineering in 2021, is a Ph.D. student of Mechanical Engineering at the University of Texas at Dallas. His research focuses on the practical application of the solar energy in the industry. Now his principal research is about solar vapor system in order to design the system which can realize the function that both has the high efficiency of vaporization below the sunlight and has the capability to reject the salt generate with the process in the vaporization.

Siyu Tian received his B. S. degree from Huazhong University of Science and Technology in 2014, M. S. degree from Huazhong University of Science and Technology in 2017. Currently he is a Ph.D. candidate of Mechanical Engineering in the Erik Jonsson School of Engineering and Computer Science at the University of Texas at Dallas. His research focuses on nanoscale heat transfer of batteries, electrochemical energy storage materials, and structure design of aerogels based on 2D materials.

Long Zhou received his B. S. degree from Sichuan University, Sichuan, China in 2017, M. S. degree from Stony Brook University, New York, the United States in 2019. Currently, he is a Ph.D. student and research assistant in Mechanical Engineering at the Erik Jonsson School of Engineering and Computer Science at the University of Texas at Dallas. His research focuses on electrochemical energy storage materials and devices and the mechanical properties of materials.

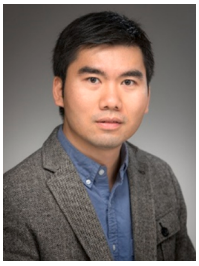

Dr. Tengfei Luo is the Dorini Family Collegiate Chair and Associate Professor in the Department of Aerospace and Mechanical Engineering (AME) at the University of Notre Dame (UND). Before joining UND, he was a postdoctoral associate at Massachusetts Institute of Technology (2009-2011) after obtaining his PhD from Michigan State University (2009). At UND, Dr. Luo leads an interdisciplinary group of PhD students, postdocs, academic visitors and undergraduate researchers, focusing on nanoscale thermal transport, electronics thermal management, novel material design and manufacturing, and water treatment.

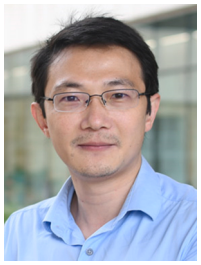

Dr. Guoping Xiong received his B. S. degree from Huazhong University of Science and Technology in 2005, M. S. degree from Tsinghua University, Beijing, China in 2008, and Ph.D. degree from Purdue University in 2013. Currently he is an Assistant Professor of Mechanical Engineering in the Erik Jonsson School of Engineering and Computer Science at the University of Texas at Dallas. His lab research focuses on solar energy harvesting, thermal management and transport, electrochemical energy storage materials and devices, and 2D materials synthesis.